Applied Surface Science 607 (2023) 154991

Contents lists available at ScienceDirect

Applied Surface Science

journal homepage: www.elsevier.com/locate/apsusc

Full Length Article

A transversal approach to predict surface charge compensation in piezoelectric force microscopy

Huan Tan [a], Jike Lyu [a], Yunwei Sheng [a], Pamela Machado [a], Tingfeng Song [a], Akash Bhatnagar [b,c,d], Mariona Coll [a], Florencio Sánchez [a], Josep Fontcuberta [a], Ignasi Fina [a,*]

[a] Institut de Ciencia de Materials de Barcelona-CSIC, Campus de la UAB, Bellaterra, Barcelona 08193, Spain
[b] Zentrum für Innovationskompetenz SiLi-nano, Martin Luther Universität Halle-Wittenberg, Halle (Saale) 06120, Germany
[c] Institute of Physics, Martin Luther Universität Halle-Wittenberg, Halle (Saale) 06120, Germany
[d] SCHOTT AG, Hattenbergstrasse 10, 55122 Mainz, Germany

ARTICLE INFO

Keywords:
Ferroelectrics
Surface chemistry
Surface charges
Piezoelectric force microscopy

ABSTRACT

Piezoelectric force microscopy (PFM) has demonstrated to be a powerful tool to characterize ferroelectric materials. However, extrinsic effects, most notably, those resulting from surface charges, often mask or mirror genuine piezoelectric response, challenging PFM data understanding. The contribution of surface charges to PFM signal is commonly compensated by using appropriate external bias voltage, which is *ad-hoc* selected and sample dependent. Here, we determine the compensating voltage in thin films of different ferroelectric materials and we compare with the corresponding *I-V* characteristics recorded using suitable electrodes. It turns out that the sign and magnitude of the bias voltage required to compensate the surface charges are related to the asymmetry of the *I-V* characteristics. We propose that this relation results from the fact that the semiconducting properties of the material determine both the *I-V* dependence, and the sign of charged adsorbates. We show how to make use of this correlation to predict the required compensation voltage of a non-ferroelectric material and we show that spurious piezoelectric-like contributions are largely cancelled. The results provide guidelines to mitigate common extrinsic contributions in PFM imaging.

1. Introduction

Since its discovery [1], scanning probe microscopy (SPM) has revolutionized the materials characterization at the nanoscale. Contrary to other surface sensitive or imaging techniques, SPM allows diverse functional characterization. In particular, piezoelectric force microscopy (PFM) has demonstrated to be a powerful tool to characterize ferroelectric materials [2–4], including polarization switching dynamics [5,6]. However, it is widely recognized that surface charges affect the PFM response signal and its interpretation might be intricate [7].

In PFM an alternating voltage signal (V_{ac}) is applied to the surface of the sample through the tip and the voltage-induced deformation of the sample is probed. The effective piezoresponse (d_{eff}) relates these two magnitudes. In any piezoelectric material, d_{eff} is affected by different contributions [8]. The first one is related to the intrinsic material piezoresponse (d). When imaging ferroelectric materials by PFM a linear deformation of the cantilever is expected if an additional external voltage (V_{dc}) is applied. At $V_{dc} = 0$, well predicted amplitude and phase responses are expected for domains with polar axis pointing in opposite direction along the normal to sample surface [2]: a constant amplitude signal for regions with polarization pointing along opposite directions with zero signal at the domain walls, and a sharp 180° phase contrast between regions with polarization pointing along opposite directions.

The second one, added to the intrinsic contribution to the deformation, results from electrostatic interactions between the PFM cantilever and charges at the surface of the material [9,10]. Surface charges lead to a potential difference ($V_{surface}$) between the sample and the cantilever that contributes to the observed deformation of the cantilever, perturbing PFM mapping [11]. As a result, a contrast of amplitude between ferroelectric domains of opposite polarization and non-180° phase contrast can be observed, being fingerprints of extrinsic contributions to the PFM response. The influence of the $V_{surface}$ term on the cantilever deformation and thus on d_{eff} depends on the capacitance (C) between the cantilever and the surface, and the spring constant of the cantilever (k). Therefore, in presence $V_{surface}$ and V_{dc}, the d_{eff} can be expressed as [11]:

* Corresponding author.
E-mail address: ifina@icmab.es (I. Fina).

https://doi.org/10.1016/j.apsusc.2022.154991
Received 1 June 2022; Received in revised form 9 September 2022; Accepted 19 September 2022
Available online 23 September 2022

$$d_{eff} = d + \left|\frac{C}{k}(V_{dc} - V_{surface})\right| \quad [1]$$

It follows that the use of stiffer cantilevers results in smaller extrinsic deformation [12,13]. However, this is not always possible because stiffer cantilevers lead also to smaller deformation and thus compromise the sensitivity. The reduction of the capacitance C is an alternative. However, modification of the microscope geometry to reduce C, for instance by modifying the length of the cantilever, is not always possible without affecting the sensitivity of the PFM instrument [13,14]. In contrast, application of compensation voltage (V_{dc}*) has been shown as a convenient and flexible method to compensate charge effects [15] without reducing the PFM sensitivity and applicable to any material. The method consists in biasing the tip while imaging with $V_{dc}^* = V_{surface}$, thus the extrinsic contribution is zeroed. Usually V_{dc}* is evaluated by guesswork trying to minimize the PFM amplitude contrast and reach 180° phase contrast between domains with opposite polarization. The method is also limited by the fact that sample biasing can result in ferroelectric switching if V_{dc}* is larger than the coercive voltage or in important charge injection [16–18]. On the other hand, it can be expected that charging effects are dependent on transport properties of the characterized material [19–21] and it could be anticipated that V_{dc}* is related to them. However, any relation between transport properties of the sample under study and the required compensating voltage V_{dc}* remains to be elucidated.

In the present work the electrical properties of the sample have been inspected by measuring the *I-V* characteristics across the film using suitable 2-probe contact configuration in a dedicated probe station. In particular, a metallic tip in direct contact to the sample under study to minimize the contribution of surface charges, is used as top electrode. The main features of the *I-V* characteristics, namely their rectifying character and the threshold voltage are compared with the V_{dc}* used for PFM imaging of different ferroelectric materials; $BaTiO_3$, $BiFeO_3$, $LuFeO_3$ and $Hf_{0.5}Zr_{0.5}O_2$. A close correspondence is identified between the observed rectifying behavior of the *I-V* characteristics and the sign and magnitude of the V_{dc}* required for optimal collection of PFM images. We argue that both properties are consequences of the transport properties of the films, namely their *n* or *p* character, and thus are related. We show that these findings can also be extended to account and compensate charging effects in PFM images of non-polar materials.

2. Experimental

Epitaxial thin films of different ferroelectric materials have been characterized. A $BaTiO_3$ (60 nm)/$La_{2/3}Sr_{1/3}MnO_3$(25 nm) bilayer was grown by pulsed laser deposition (PLD) in a single process on top of a LSAT(001) substrate [22]. An hexagonal $LuFeO_3$ (60 nm) film was grown by PLD on Pt (20 nm) buffered sapphire substrates [23]. A $BiFeO_3$ (90 nm)/$La_{2/3}Sr_{1/3}MnO_3$(25 nm) bilayer was grown by chemical solution deposition [24], and a $Hf_{0.5}Zr_{0.5}O_2$ (10 nm)/$La_{2/3}Sr_{1/3}MnO_3$(25 nm) bilayer was grown by PLD [25]. Further experimental details of the deposition conditions can be found in the indicated references. The four samples are sketched in Fig. 1(a,b,c,d). In addition, a 5 % Nb-doped $SrTiO_3$ single-crystal and a Si wafer with native SiO_2 were also characterized. X-ray diffraction (XRD) patterns were collected with Cu-Kα radiation using a Siemens D5000 diffractometer equipped with a point detector. PFM measurements were performed with an MFP-3D microscope (Oxford Instrument Co.) using BudgetSensors silicon (*n*-type) cantilevers with Pt coating (Multi75E-G). To enhance sensitivity, the dual AC resonance tracking (DART) method was employed [26]. The selected measurement frequency is ± 5 % off the resonance. PFM voltage-displacement hysteresis loops were always collected at remanence (without applying bias voltage) using a dwell time of 100 ms after applying the voltage pulse of the indicated amplitude. PFM loops are in Supplementary Material S1. Due to the limitations of DART mode to quantify PFM response [27], we do not address here the quantitative determination of the piezoelectric coefficients, although all the measurements in all samples are done under the same conditions, making them comparable. *I-V* characteristics have been performed using the 6517B electrometer (Keithley Co.) with a biased 5 μm tip directly pressed into the bare surface of the film while grounding the bottom electrode. This set up allows to obtain large values of current, reducing the noise, and minimizing the contribution of surface charges to the recorded *I-V*'s. In PFM and *I-V* characterization LSMO was used as a bottom electrode for the $BaTiO_3$, $BiFeO_3$, and $Hf_{0.5}Zr_{0.5}O_2$ samples and Pt for the $LuFeO_3$ one. In the case of the Nb-doped $SrTiO_3$ single-crystal and SiO_2, Ag-paste covering the backside of the Nb:$SrTiO_3$ crystal and Si were used as ground bottom electrodes, respectively.

3. Results

θ-2θ scans shown in Fig. 1(e,f,g,h) indicate that all the films are crystalline with (001) texture for $BaTiO_3$ (001) texture for hexagonal LuFeO3, (0001) texture for $BiFeO_3$, and (111) texture for $Hf_{0.5}Zr_{0.5}O_2$. In fact, all the samples are epitaxial as shown elsewhere [22–25]. The bottom electrode ($La_{2/3}Sr_{1/}3MnO_3$ for $BaTiO_3$, $BiFeO_3$, and $Hf_{0.5}Zr_{0.5}O_2$ and Pt for $LuFeO_3$) and substrate reflections are indicated in the θ-2θ scans.

First, we focus on PFM characterization of an archetypical ferroelectric material: $BaTiO_3$. Fig. 2(a,b) show PFM images (amplitude and phase, respectively) collected after applying ± 8 V on the bare surface of the $BaTiO_3$ film [sketch in inset of Fig. 2(a)]. In both figures, the brighter regions correspond to regions written with −8 V (with polarization

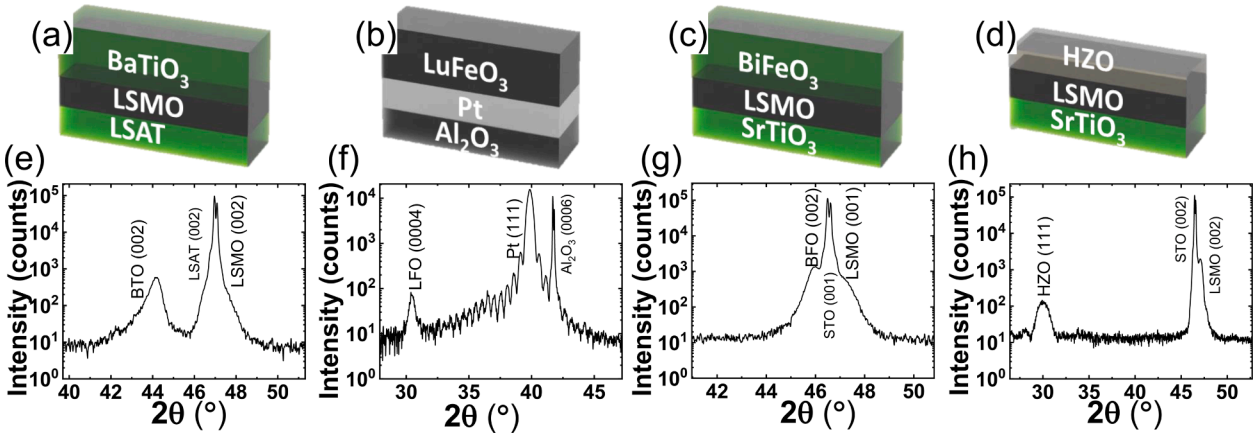

Fig. 1. (a,b,c,d) Sketches of the samples: $BaTiO_3$, $LuFeO_3$, $BiFeO_3$ and $Hf_{0.5}Zr_{0.5}O_2$, respectively (e,f,g,h) θ-2θ scans shown for $BaTiO_3$, $LuFeO_3$, $BiFeO_3$ and $Hf_{0.5}Zr_{0.5}O_2$ films, respectively.

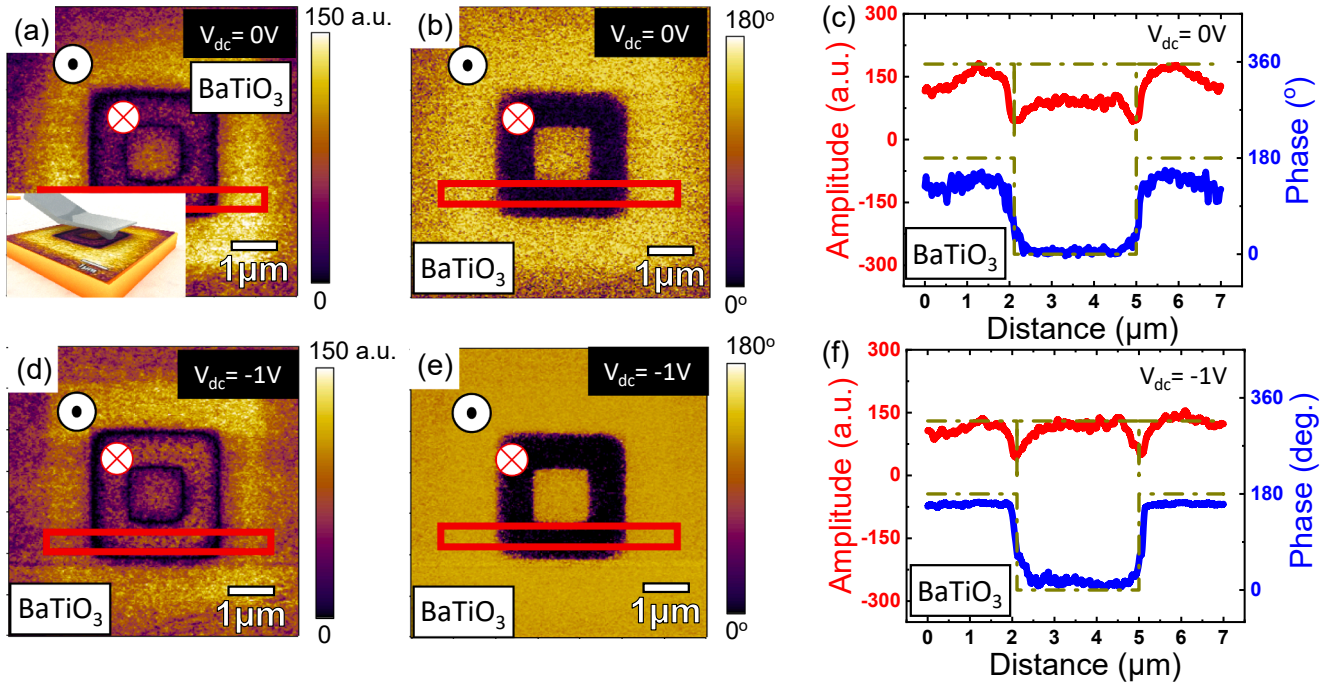

Fig. 2. PFM (a) amplitude and (b) phase images of $BaTiO_3$ film. (c) PFM amplitude and phase profiles corresponding to the region enclosed by a red rectangle in panels (a,b). PFM (d) amplitude and (e) phase images of $BaTiO_3$ film obtained during the application of $V_{dc} = -1$ V to the tip. (f) PFM amplitude and phase profiles corresponding to the region enclosed by a red rectangle in panels (d,e). Outwards and inwards symbols indicate the direction of the ferroelectric polarization.

upwards as indicated by the doted circle in the figure) and the darker written with + 8 V (with polarization downwards as indicated by the crossed circle). The PFM amplitude image [Fig. 2(a)] shows a contrast of amplitude between positive and negative biased regions. There is also a phase contrast in the same areas in Fig. 2(b).

The phase profile [blue line in Fig. 2(c)] shows that the phase contrast is not 180° but smaller, and the amplitude profile [red line in Fig. 2(c)] also displays a perceptible variation. As mentioned, the fact that the amplitude is not constant and the phase contrast between regions polarized by voltage of opposite sign is not 180° are clear signatures that charging effects hide the genuine ferroelectric response [expected shapes for amplitude and phase intrinsic ferroelectric contribution are indicated by dashed lines in Fig. 2(c)]. Thus, it can be concluded that the signals in Fig. 2(a-c) do not result exclusively from the ferroelectric character of the sample.

Fig. 2(d,e) shows PFM images collected while biasing the sample with V_{dc} = -1 V applied to the tip. A clear decrease of the amplitude contrast among differently poled regions and a perceptible increase of the phase contrast are observed. The corresponding average profiles [Fig. 2(f)] reveal that, except at the boundary regions, the amplitude is constant and that the phase contrast is closer to 180° for regions with opposite polarization. PFM images collected using different bias voltages V_{dc} allow to determine the dependence of the amplitude and phase contrast between regions with polarization up (↑) and down (↓) as a function of V_{dc} [Fig. 3(a,b)]. The corresponding PFM images are shown in Supplementary Material S2. It can be observed that amplitude difference minimize at $V_{dc} \approx$ -1 V (dashed lines). Similarly, phase difference is near 180° at $V_{dc} \approx$ -1 V (dashed lines). It follows that $V_{dc} \approx$ -1 V is required to achieve change compensation whereas application of larger or smaller voltages results in infra or over compensation.

Electrostatic charging of surfaces depends on the electronic properties of the materials [28,29]. Accordingly, it has to be expected that V_{dc}* reflects the electrical properties of the bulk of the films under study. We asses this expectation by characterizing different ferroelectric materials. In Fig. 4, we summarize results obtained from $LuFeO_3$, $BiFeO_3$, and $Hf_{0.5}Zr_{0.5}O_2$ films. Fig. 4(a,b) show the PFM amplitude and phase images collected with an unbiased tip (V_{dc} = 0 V), on the $LuFeO_3$ film after suitable poling with ± 8 V. PFM amplitude and phase profiles

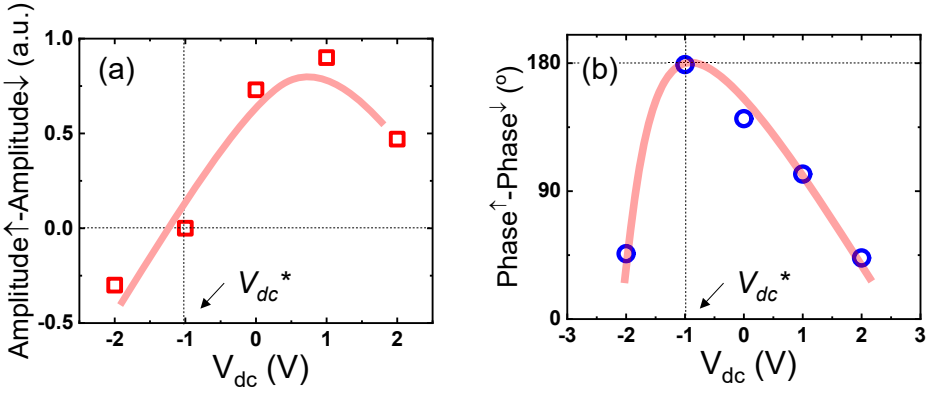

Fig. 3. PFM (a) amplitude and (b) phase images of $BaTiO_3$ film dependence on V_{dc}.

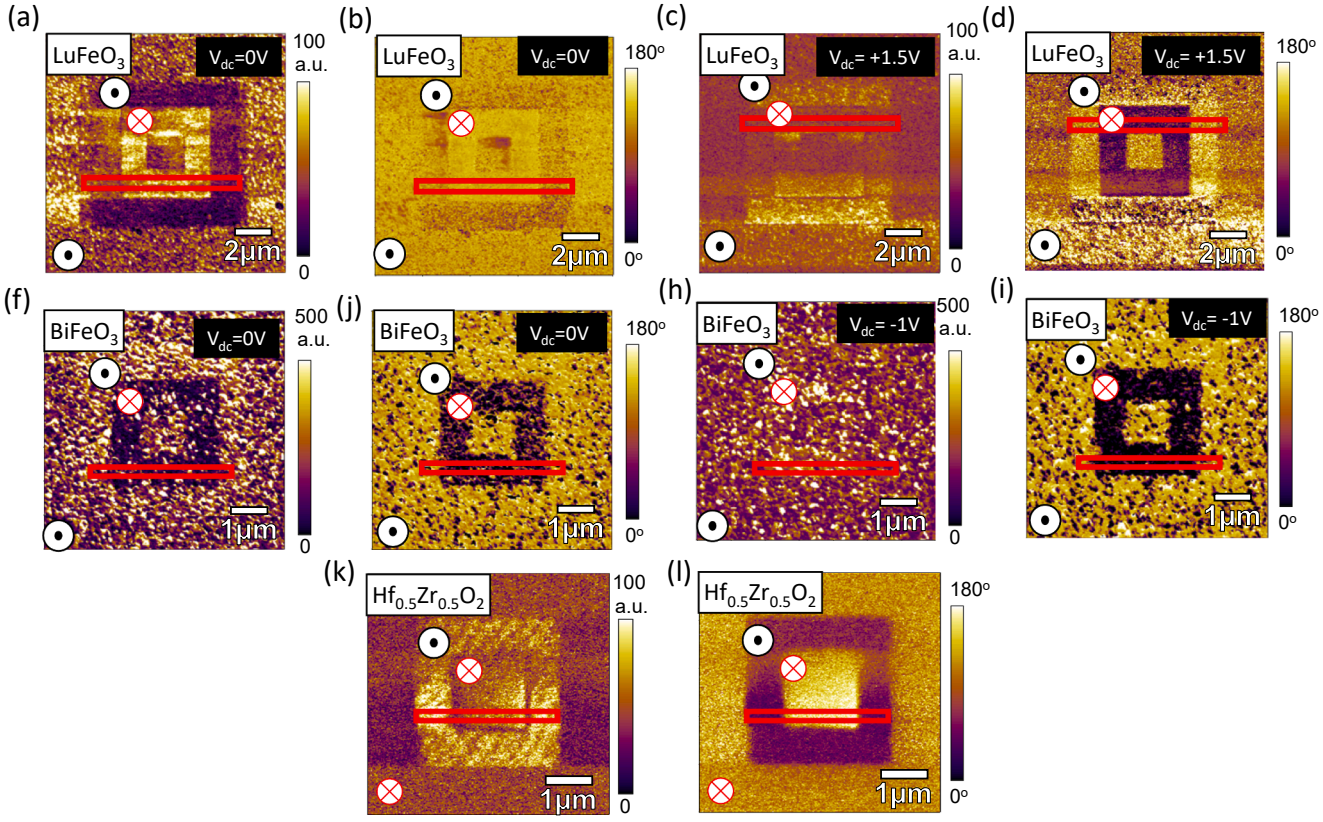

Fig. 4. PFM (a) amplitude and (b) phase images for $LuFeO_3$. (c,d) Idem obtained during the application of $V_{dc} = +1.5$ V to the tip. PFM (a) amplitude and (b) phase images for $BiFeO_3$. (g,h) Idem obtained during the application of $V_{dc} = -1$ V to the tip. PFM (i) amplitude and (j) phase images for $Hf_{0.5}Zr_{0.5}O_2$.

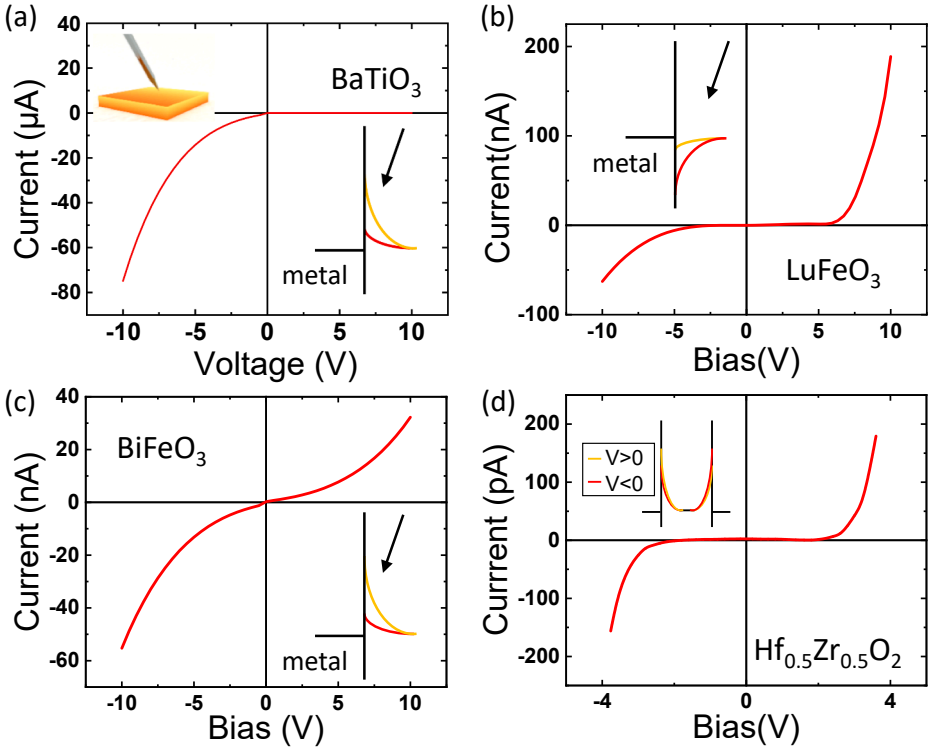

Fig. 5. (a,b,c,d) *I-V* characteristics for for $BaTiO_3$, $LuFeO_3$, $BiFeO_3$ and $Hf_{0.5}Zr_{0.5}O_2$ films, respectively. Sketches: (a) (top) illustrates the tip arrangement for top–bottom *I-V* measurements; (a,b,c,d) indicate the relative position of the Fermi level of the metal and the valence band of $LuFeO_3$ and conduction band of $BiFeO_3$ and $Hf_{0.5}Zr_{0.5}O_2$, for $V > 0$ (yellow) and $V < 0$ (red) applied to the top (right) electrode. For convenience the bottom metal/ferroelectric junction has been plotted.

corresponding to the region enclosed by a red rectangle of all the samples in Fig. 4 are shown in Supplementary Material Figure S3. It is obvious that neither the amplitude image nor the phase image are those expected for a ferroelectric material. Interestingly, as illustrated in Fig. 4 (c,d), when biasing the tip with $V_{dc} = +1.5$ V, the amplitude contrast washes out and a 180° phase contrast develops among ↑ and ↓ written regions, as expected from the ferroelectric nature of $LuFeO_3$. Therefore, the $V_{dc} = +1.5$ V bias required to compensate surface charging in $LuFeO_3$, has an opposite sign to that used for the $BaTiO_3$ film.

Similar PFM data have been collected from the $BiFeO_3$ film using an unbiased tip ($V_{dc} = 0$ V) [Fig. 4(e,f)] and a bias of $V_{dc} = -1$ V [Fig. 4 (g, h)]. It can be appreciated that the obvious contrast in the amplitude image collected at $V_{dc} = 0$ V [Fig. 4(e)] is drastically reduced under $V_{dc} = -1$ V [Fig. 4 (g)]. Note that the signal reduction at the domain wall is difficult to discern due to it is partially affected by the rougher topography of this sample. A zoomed region and profile are shown in Supplementary Material Figure S3(e). The phase contrast is also clearly improved [compare Fig. 4(f) and 4(h)]. Therefore, $V_c = -1$ V mitigates the impact of surface charges in PFM images of $BiFeO_3$. Notice that the required bias voltage has the same sign than in $BaTiO_3$ but opposite to $LuFeO_3$. Finally, for $Hf_{0.5}Zr_{0.5}O_2$ film, the contrast of amplitude among regions differently poled is found to be negligible and the phase contrast is already ≈ 180° [Fig. 4(i,j)] when using an unbiased tip ($V_{dc} = 0$ V). Thus, for for $Hf_{0.5}Zr_{0.5}O_2$ film extrinsic effects are of lesser relevance. Note than in the studied samples V_{dc}* is smaller than coercive voltage (at 2 V or above for the studied films as inferred from the loops shown in Supporting Information Figure S1). Therefore, switching of ferroelectric regions is not relevant while imaging in the characterized samples.

To gain a further insight into the origin of the required different V_{dc}* in different materials, *I-V* characteristics are measured by placing a 5 μm tip on the bare surface of the films [sketch in inset of Fig. 5(a)], while the bottom electrode is grounded. We have used a 5 μm tip to mimic the configuration used in the PFM but with larger contact area thus larger values of current with reduced noise are collected, and the contribution of charging effects in the *I-V* measurements is minimized. Fig. 5(a) shows the *I-V* characteristics measured on $BaTiO_3$. It can be observed that the current is larger for negative applied voltage. This rectifying behavior is a signature of the presence of a Schottky barrier or related rectifying contact. The *I-V* curve recorded on the $LuFeO_3$ film is shown in Fig. 5(b). Data shows that, the $LuFeO_3$ film is more resistive than $BaTiO_3$ but, of higher interest is the observation that the conductivity for positive bias is greater than for negative. Thus, the rectifying response of $LuFeO_3$ is opposite to that of $BaTiO_3$. In addition, the onset positive voltage at which $LuFeO_3$ film starts to conduct (≈ 6 V) is larger than in $BaTiO_3$ (≈ |-2 V|). For $BiFeO_3$ [Fig. 5(c)], the rectifying behavior is not as pronounced as in $BaTiO_3$ [Fig. 5(a)], but a larger conductance occurs for $V < 0$. This observation indicates the presence of a predominant interface energy barrier of the same sign as that observed in $BaTiO_3$ [Fig. 5(a)] which fingerprints the presence of a similar rectifying behavior, but opposite to $LuFeO_3$. The *I-V* characteristics for $Hf_{0.5}Zr_{0.5}O_2$ [Fig. 5(d)] has been collected at smaller voltage range (< |4 V|) to minimize the contribution of ionic motion, which is known to be prominent in hafnium oxide films [30]. Data indicate a symmetric *I-V* behavior and a low conductivity, consistent with the large bandgap of HZO. Therefore, a correlation between the V_{dc}* and the asymmetry in *I-V* characteristic has been identified in different materials as summarized in Table I.

The rectifying nature of a metal/semiconductor contact, shortly attributed here to a Schottky barrier, is primarily determined by the type of conductivity of the semiconductor (*n* or *p*-type), its electron affinity and the work functions of the electrodes. $BaTiO_3$ is typically found to be an *n*-type semiconductor [31,32], whereas in $BiFeO_3$ *n*-type and *p*-type behavior can be easily accommodated either by oxygen vacancies or cationic non-stoichiometry [33,34]. The more open structure of $LuFeO_3$ allows interstitial oxygen ions that promote a *p*-type electronic conductivity [35]. Consistently, metal/*n*-type [Fig. 5(a,c)] or metal/*p*-type [Fig. 5(b)] barriers are observed in $BaTiO_3$ and $BiFeO_3$, and $LuFeO_3$, respectively. Therefore, the rectifying behavior is observed to be reversed in these set of films. The relatively less abundant defect density and the larger band gap of HZO anticipate minor shift of the Fermi level respect to the intrinsic one, neither at the bulk nor at any interface, resulting in symmetric behavior [Fig. 5(d)]. Besides, the electronic nature of the material determines the sign of the charges available at its surface and therefore the surface electrostatic potential [28]. For *n*-type semiconductor, positive charging and a concomitant potential increase is more likely to occur [Fig. 6(a)]. The opposite scenario would hold for *p*-type material [Fig. 6(b)] [28]. This results from the fact that in *n*-type (*p*-type) semiconductors negatively (positively) charged states are expected and these can be partially compensated by positive (negative) charges attracted to the surface. In brief, depending on the *n* or *p* character of the material under exploration, V_{dc}* of different sign would be required to compensate charging effects. This agrees with the results summarized in Table 1, the V_{dc}* sign is opposite to the rectifying polarity extracted from the *I-V* curve. Therefore, the semiconducting properties of the ferroelectric layer determines the band bending at the top electrode interface and determines the surface charge trapping and consequently V_{dc}*.

To further assess these findings and aiming to predict V_{dc}* on the basis of the *I-V* curve asymmetry, we explored the PFM images of Nb(0.5 %):$SrTiO_3$ single crystals, where Nb-doping induces a metallic behavior. In Fig. 7(a), we show the hysteresis loops measured at the surface of a Nb:$SrTiO_3$ crystal. The amplitude and phase loops show a butterfly loop and near 170° phase contrast, respectively. These can be taken as signature of the ferroelectric nature of the material, although Nb:$SrTiO_3$ is definitely not. The corresponding *I-V* characteristics [Fig. 7(b)], indicates a strong rectifying behavior of the tip/Nb:$SrTiO_3$ sample, which conducts for $V > 0$. Note that Nb:$SrTiO_3$ is *n*-type semiconductor but rectifies for opposite polarity than $BaTiO_3$, probably related to the different metallic bottom electrodes used (Ag-paste for Nb:$SrTiO_3$ and LSMO for $BaTiO_3$). The sample is subsequently written with $V = \pm 8$ V and the corresponding amplitude and phase PFM images are collected with $V_{dc} = 0$ V [Fig. 7(c,d)]. The amplitude map does not show any perceptible contrast [Fig. 7(c)] but a large phase contrast (≈ 40°) can be observed [Fig. 7(d)]. Similar response is observed in other non-ferroelectric materials such as Al_2O_3 [36]. At first sight, the shape of the PFM loops [Fig. 7(a)], the absence of amplitude contrast [Fig. 7(c)] and the presence of phase contrast [Fig. 7(d)] could be attributed to a ferroelectric character of the sample. However, the origin of the hysteresis in the PFM loops and phase contrast in the PFM phase image can be divers, f.i. charge injection, oxygen vacancies, electrostatic effect, etc. [16–18]. From the analysis of the asymmetry of the *I-V* of Fig. 7(a), we can expect that V_{dc}* > 0 would be required to compensate possible extrinsic effects. Indeed, in Fig. 7(e,f) we show the amplitude and phase images obtained using $V_{dc} = +1$ V. It is obvious that the phase contrast has been largely suppressed, denying any ferroelectric character or the sample. Therefore, transport characterization has been helpful on predicting V_{dc}* and, therefore, to assess the intrinsic non-ferroelectric properties of the Nb:STO_3 sample by PFM. Similar crosschecking experiments have been performed on SiO_2 films, with consistent results (Supplementary Material S4).

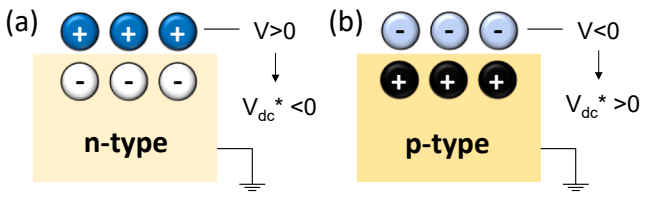

Fig. 6. (a) Sketch of the sign of accumulated charges in a *n*-type semiconductor and the generated voltage increase. (b) Idem for a *p*-type semiconductor and the generated voltage decrease.

Table 1
Summary of the V_{dc}* used to cancel the amplitude contrast and to obtain a 180° phase contrast in the PFM images, respectively, and the rectifying branch polarity for the characterized samples.

	$BaTiO_3$	$LuFeO_3$	$BiFeO_3$	$Hf_{0.5}Zr_{0.5}O_2$
V_{dc}* (V)	−1	+1.5	−1	0
Rectifying polarity	Positive	Negative	Positive	None

4. Conclusions

PFM images and *I-V* characteristics measurements of different ferroelectric oxide films with different electric properties have been reported. It is observed that sample charging effects on PFM images can be compensated by V_{dc}* of the opposite polarity to the rectifying polarity identified in *I-V* characteristics collected using simple tip-on-sample experiment. We argue that the disclosed relation between the required voltage to compensate surface charging effects and the rectifying nature of the tip-film interface, is a consequence of the impact of semiconducting properties of the material, namely its *p*- or *n*-type character, on the band bending and on the sign of adsorbates. Although available data does not allow to stablish a causal link among these two phenomena, the observed correlation provides a useful tool to determine the polarity of V_{dc} required to compensate extrinsic contributions in the PFM signal in dielectric thin films. Thus, extrinsic responses resembling and somehow masking genuine ferroelectric contributions can be removed. These findings might be useful to fix the ideal experimental conditions for PFM characterization minimizing spurious non-ferroelectric contributions and should be useful for any ferroelectric or non-ferroelectric material rather than limited to the materials explored in the present work.

CRediT authorship contribution statement

Huan Tan: Investigation. **Jike Lyu:** Investigation. **Yunwei Sheng:** Investigation. **Pamela Machado:** Investigation. **Tingfeng Song:** Investigation. **Akash Bhatnagar:** Investigation. **Mariona Coll:** Investigation. **Florencio Sánchez:** Investigation, Conceptualization. **Josep Fontcuberta:** Investigation, Conceptualization. **Ignasi Fina:** Investigation, Conceptualization.

Declaration of Competing Interest

The authors declare that they have no known competing financial

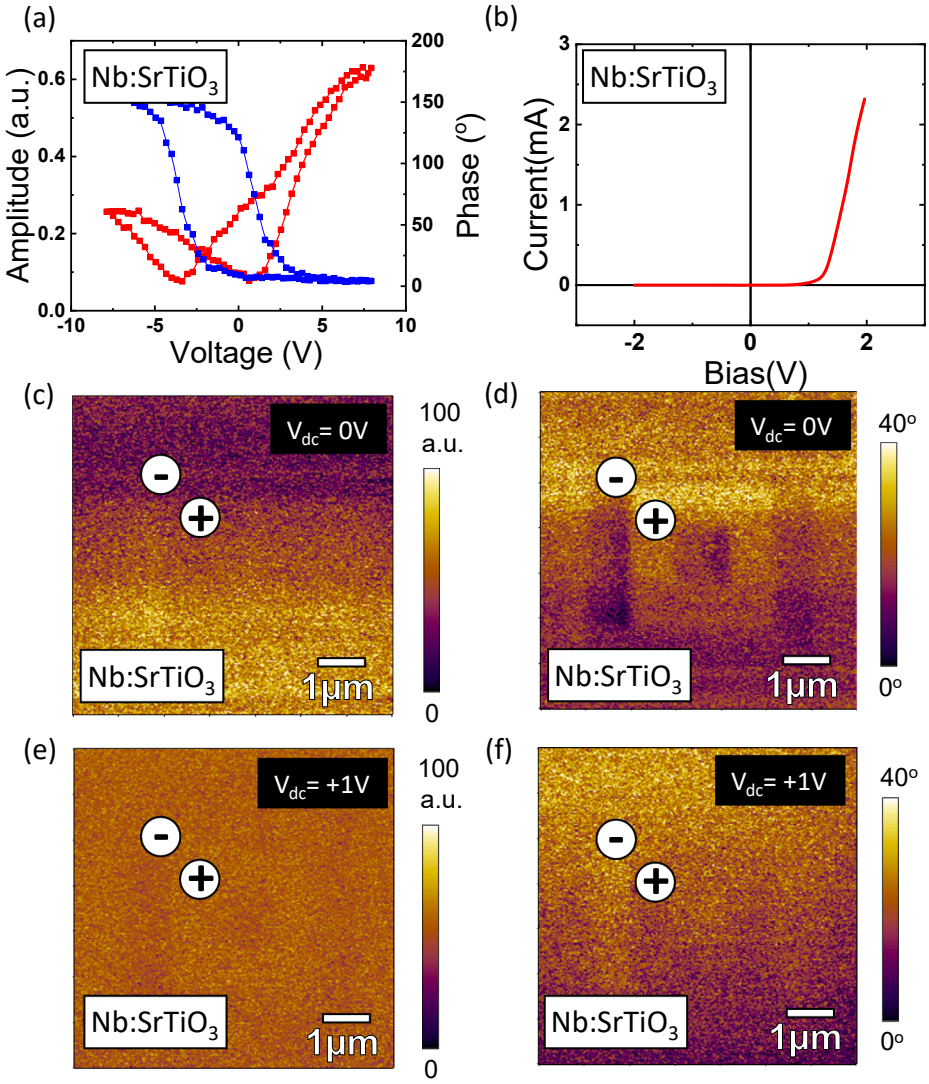

Fig. 7. (a) PFM amplitude and phase hysteresis loops for Nb:$SrTiO_3$. (b) The *I-V* characteristics for Nb:$SrTiO_3$. PFM (c) amplitude and (d) phase images without V_{dc}. PFM (e) amplitude and (f) phase images are obtained during the application of $V_{dc} = +1$ V to the tip. + and – symbols indicate the regions where + 8 or −8 V were applied to the tip prior the measurement.

interests or personal relationships that could have appeared to influence the work reported in this paper.

Data availability

Data will be made available on request.

Acknowledgments

Financial support from the Spanish Ministry of Science and Innovation (10.13039/501100011033), through the Severo Ochoa FUNFUTURE (project CEX2019-000917-S funded by MCIN/AEI), project TED2021-130453B-C21 funded by MCIN/AEI and European Union NextGenerationEU/PRTR, and projects PID2020-118479RB-I00, PID2020-112548RB-I00, PID2020-114224RB-I00 and PID2019-107727RB-I00 funded by MCIN/AEI, and from CSIC through the i-LINK (LINKA20338) program are acknowledged. Project supported by a 2020 Leonardo Grant for Researchers and Cultural Creators, BBVA Foundation. HT, TS and YS are financially supported by China Scholarship Council (CSC) with No. 201906050014, 201807000104, and 201806410010. PM is financially supported by FPI fellowship PRE2018-084618. The work of HT, TS, PM and YS has been done as a part of their Ph.D. program in Materials Science at Universitat Autònoma de Barcelona.

Appendix A. Supplementary data

Supplementary data to this article can be found online at https://doi.org/10.1016/j.apsusc.2022.154991.

References

[1] G. Binnig, C.F. Quate, C. Gerber, Atomic force microscope, Phys. Rev. Lett. 56 (1986) 930.
[2] M. Alexe, A. Gruverman, Nanoscale characterisation of ferroelectric materials: scanning probe microscopy approach, Springer Science & Business Media, 2004.
[3] S.V. Kalinin, A. Rar, S. Jesse, A decade of piezoresponse force microscopy: progress, challenges, and opportunities, IEEE Trans. Ultrason. Ferroelectr. Freq. Control 53 (2006) 2226–2252.
[4] S.V. Kalinin, B.J. Rodriguez, S. Jesse, E. Karapetian, B. Mirman, E.A. Eliseev, A. N. Morozovska, Nanoscale electromechanics of ferroelectric and biological systems: a new dimension in scanning probe microscopy, Annu. Rev. Mater. Res. 37 (2007) 189–238.
[5] S.V. Kalinin, A.N. Morozovska, L.Q. Chen, B.J. Rodriguez, Local polarization dynamics in ferroelectric materials, Rep. Prog. Phys. 73 (2010), 056502.
[6] S.V. Kalinin, S. Jesse, B.J. Rodriguez, K. Seal, A.P. Baddorf, T. Zhao, Y. Chu, R. Ramesh, E.A. Eliseev, A.N. Morozovska, Recent advances in electromechanical imaging on the nanometer scale: Polarization dynamics in ferroelectrics, biopolymers, and liquid imaging, Jpn. J. Appl. Phys. 46 (2007) 5674.
[7] R.K. Vasudevan, S. Zhang, M.B. Okatan, S. Jesse, S.V. Kalinin, N. Bassiri-Gharb, Multidimensional dynamic piezoresponse measurements: Unraveling local relaxation behavior in relaxor-ferroelectrics via big data, J. Appl. Phys., 118 (2015) 072003.
[8] D. Seol, B. Kim, Y. Kim, Non-piezoelectric effects in piezoresponse force microscopy, Curr. Appl Phys. 17 (2017) 661–674.
[9] S.V. Kalinin, D.A. Bonnell, Artifacts and Non-Local Effects in SPM Potential Measurements, Microscopy Today 10 (2002) 16–21.
[10] N. Balke, S. Jesse, P. Yu, B. Carmichael, S.V. Kalinin, A. Tselev, Quantification of surface displacements and electromechanical phenomena via dynamic atomic force microscopy, Nanotechnology 27 (2016), 425707.
[11] N. Balke, S. Jesse, Q. Li, P. Maksymovych, M. Baris Okatan, E. Strelcov, A. Tselev, S.V. Kalinin, Current and surface charge modified hysteresis loops in ferroelectric thin films, J. Appl. Phys., 118 (2015) 072013.
[12] J. Christman, H. Maiwa, S.-H. Kim, A. Kingon, R. Nemanich, Piezoelectric measurements with atomic force microscopy, Appl. Phys. Lett. 73 (1998) 3851.
[13] A. Gomez, T. Puig, X. Obradors, Diminish electrostatic in piezoresponse force microscopy through longer or ultra-stiff tips, Appl. Surf. Sci. 439 (2018) 577–582.
[14] J. Virtanen, V. Sariola, S. Tuukkanen, Piezoelectric cantilever force sensor sensitivity measurements, J. Phys. Conf. Ser. 1065 (2018), 042005.
[15] S. Kim, D. Seol, X. Lu, M. Alexe, Y. Kim, Electrostatic-free piezoresponse force microscopy, Sci. Rep. 7 (2017) 41657.
[16] N. Balke, P. Maksymovych, S. Jesse, I.I. Kravchenko, Q. Li, S.V. Kalinin, Exploring Local Electrostatic Effects with Scanning Probe Microscopy: Implications for Piezoresponse Force Microscopy and Triboelectricity, ACS Nano 8 (2014) 10229–10236.
[17] N. Balke, P. Maksymovych, S. Jesse, A. Herklotz, A. Tselev, C.-B. Eom, I. I. Kravchenko, P. Yu, S.V. Kalinin, Differentiating Ferroelectric and Nonferroelectric Electromechanical Effects with Scanning Probe Microscopy, ACS Nano 9 (2015) 6484–6492.
[18] M. Andrä, F. Gunkel, C. Bäumer, C. Xu, R. Dittmann, R. Waser, The influence of the local oxygen vacancy concentration on the piezoresponse of strontium titanate thin films, Nanoscale 7 (2015) 14351–14357.
[19] V.W. Ballarotto, K. Siegrist, R.J. Phaneuf, E.D. Williams, S. Mogren, PEEM imaging of dopant contrast in Si(001), Surf. Sci. 461 (2000). L570–L574.
[20] V.W. Ballarotto, M. Breban, K. Siegrist, R.J. Phaneuf, E.D. Williams, Photoelectron emission microscopy of ultrathin oxide covered devices, J. Vac. Sci. Technol. B: Microelectron. Nanometer Struct. Process., Measur., Phenomena 20 (2002) 2514–2518.
[21] M. Lavayssière, M. Escher, O. Renault, D. Mariolle, N. Barrett, Electrical and physical topography in energy-filtered photoelectron emission microscopy of two-dimensional silicon pn junctions, J. Electron. Spectrosc. Relat. Phenom. 186 (2013) 30–38.
[22] M. Scigaj, C.H. Chao, J. Gazquez, I. Fina, R. Moalla, G. Saint-Girons, M. F. Chisholm, G. Herranz, J. Fontcuberta, R. Bachelet, F. Sanchez, High ferroelectric polarization in c-oriented $BaTiO_3$ epitaxial thin films on $SrTiO_3$/Si(001), Appl. Phys. Lett. 109 (2016) 4.
[23] Y. Sheng et al., To be published. , in, 2021.
[24] P. Machado, M. Scigaj, J. Gazquez, E. Rueda, A. Sanchez-Diaz, I. Fina, M. Gibert-Roca, T. Puig, X. Obradors, M. Campoy-Quiles, M. Coll, Band Gap Tuning of Solution-Processed Ferroelectric Perovskite $BiFe_{1-x}Co_xO_3$ Thin Films, Chem. Mater. 31 (2019) 947–954.
[25] J. Lyu, I. Fina, R. Solanas, J. Fontcuberta, F. Sánchez, Robust ferroelectricity in epitaxial $Hf_{1/2}Zr_{1/2}O_2$ thin films, Appl. Phys. Lett. 113 (2018), 082902.
[26] B.J. Rodriguez, C. Callahan, S.V. Kalinin, R. Proksch, Dual-frequency resonance-tracking atomic force microscopy, Nanotechnology 18 (2007), 475504.
[27] S.M. Neumayer, S. Saremi, L.W. Martin, L. Collins, A. Tselev, S. Jesse, S.V. Kalinin, N. Balke, Piezoresponse amplitude and phase quantified for electromechanical characterization, J. Appl. Phys. 128 (2020), 171105.
[28] T. Nakamura, N. Ishida, K. Sagisaka, Y. Koide, Surface potential imaging and characterizations of a GaN p-n junction with Kelvin probe force microscopy, AIP Adv. 10 (2020), 085010.
[29] M. DeJarld, P.M. Campbell, A.L. Friedman, M. Currie, R.L. Myers-Ward, A.K. Boyd, S.G. Rosenberg, S.P. Pavunny, K.M. Daniels, D.K. Gaskill, Surface potential and thin film quality of low work function metals on epitaxial graphene, Sci. Rep. 8 (2018) 16487.
[30] M. Lanza, A Review on Resistive Switching in High-k Dielectrics: A Nanoscale Point of View Using Conductive Atomic Force Microscope, Materials 7 (2014) 2155–2182.
[31] N.G. Eror, D.M. Smyth, Nonstoichiometric disorder in single-crystalline $BaTiO_3$ at elevated temperatures, J. Solid State Chem. 24 (1978) 235–244.
[32] C.-R. Song, H.-I. Yoo, Chemical diffusivity of BaTiO3−δ: I. Experimental determination, Solid State Ionics 120 (1999) 141–153.
[33] T.R. Paudel, S.S. Jaswal, E.Y. Tsymbal, Intrinsic defects in multiferroic $BiFeO_3$ and their effect on magnetism, Phys. Rev. B 85 (2012), 104409.
[34] L. You, N.T. Chua, K. Yao, L. Chen, J. Wang, Influence of oxygen pressure on the ferroelectric properties of epitaxial $BiFeO_3$ thin films by pulsed laser deposition, Phys. Rev. B 80 (2009), 024105.
[35] S.H. Skjærvø, E.T. Wefring, S.K. Nesdal, N.H. Gaukås, G.H. Olsen, J. Glaum, T. Tybell, S.M. Selbach, Interstitial oxygen as a source of p-type conductivity in hexagonal manganites, Nat. Commun. 7 (2016) 1–8.
[36] Z. Guan, Z.-Z. Jiang, B.-B. Tian, Y.-P. Zhu, P.-H. Xiang, N. Zhong, C.-G. Duan, J.-H. Chu, Identifying intrinsic ferroelectricity of thin film with piezoresponse force microscopy, AIP Adv. 7 (2017), 095116.